ORIGINAL RESEARCH

Phosphotungstate Acid Doped Polyanilines Nanorods for in situ NIR-II Photothermal Therapy of Orthotopic Hepatocellular Carcinoma in Rabbit

Chen Tian [ID][1],*, XiaoLei Xue[2],*, Ye Chen[3],*, Ruiyuan Liu [ID][4], Yutong Wang [ID][5], Sheng Ye[4], Zeyu Fu[5], Yingrui Luo [ID][5], Shengmiao Wang[5], Xiaofeng He[1], Huajin Pang [ID][1]

[1]Division of Vascular and Interventional Radiology, Department of General Surgery, Nanfang Hospital, Southern Medical University, Guangzhou, Guangdong, 510515, People's Republic of China; [2]Department Pathology, Nanfang Hospital, Southern Medical University, Guangzhou, Guangdong, 510515, People's Republic of China; [3]Laboratory of Interventional Radiology, Department of Minimally Invasive Interventional Radiology and Department of Radiology, The Second Affiliated Hospital, Guangzhou Medical University, Guangzhou, Guangdong Province, 510260, People's Republic of China; [4]Guangdong Provincial Key Laboratory of Medical Image Processing, School of BioMedical Engineering, Southern Medical University, Guangzhou, Guangdong, 510515, People's Republic of China; [5]Cancer Research Institute, Experimental Education/Administration Center, School of Basic Medical Sciences, Southern Medical University, Guangzhou, Guangdong, 510515, People's Republic of China

*These authors contributed equally to this work

Correspondence: Xiaofeng He; Huajin Pang, Tel +86 13760661610, Email ozonetherapy@126.com; nfyyphj@163.com

Introduction: Second near-infrared photothermal therapy (NIR-II PTT) has become a promising strategy for treating cancer in terms of safety and potency. However, the application of NIR-II PTT was limited in the treatment of deep-buried solid tumors due to the low dose of NIR-II absorption nanomaterials and the inadequate laser energy in the deep tumor.

Methods: Herein, the authors report the engineering of NIR-II absorbing polyaniline nanorods, termed HPW@PANI Nanorods, for in situ NIR-II PTT based on optical fibers transmission of laser power and transarterial infusion for the treatment of orthotopic hepatocellular carcinoma in the rabbit. HPW@PANI Nanorods were prepared via chemical oxidant polymerization of aniline under phosphotungstic acid, which exhibited effective NIR-II absorption for hyperthermia ablation cells.

Results: HPW@PANI Nanorods were fast and efficiently deposited into primary orthotopic transplantation VX2 tumor in rabbits via transarterial infusion. Furthermore, an optical fiber was interventionally inserted into the primary VX2 tumor to transmit 1064nm laser energy for in situ NIR-II PTT, which could ablate primary tumor, inhibit distant tumor, and suppress peritoneal metastasis.

Conclusion: This study provides new insights into the application of in situ NIR-II PTT based on optical fibers transmission of laser power and transarterial injection of NIR-II absorption nanomaterials to treat deep-buried tumors.

Keywords: NIR-II absorption nanomaterials, orthotopic animal model, transarterial infusion, optical fiber transmission of laser power, deep-buried tumors

Introduction

Second near-infrared (NIR-II, 1000~1700 nm) light-activated photothermal therapy (NIR-II PTT) is an emerging tumor treatment method, which utilizes NIR-II absorbing nanomaterials to convert photon energy into hyperthermia for tumor ablation and exhibits low toxicity, small photon scattering, and high maximum permissible exposure (MPE, 1064 nm: 1 W/cm^2).[1–3] However, the application of NIR-II PTT in the treatment of deep-buried solid tumors was limited due to the low concentration of NIR-II absorption nanomaterials in solid tumors and the inadequate laser energy near the tumor tissues.

To treat the deep-buried carcinoma in situ, NIR-II absorbing nanomaterials were administrated via intravascular injection and deposited into tumor via EPR effect or targeting ligand mediation effect.[4–6] However, long accumulation time and low tumor uptake efficiency reduced therapeutic effect due to the excretion by the reticuloendothelial system during systemic circulation. Of these, transarterial infusion provides an optional approach to rapidly and efficiently

Graphical Abstract
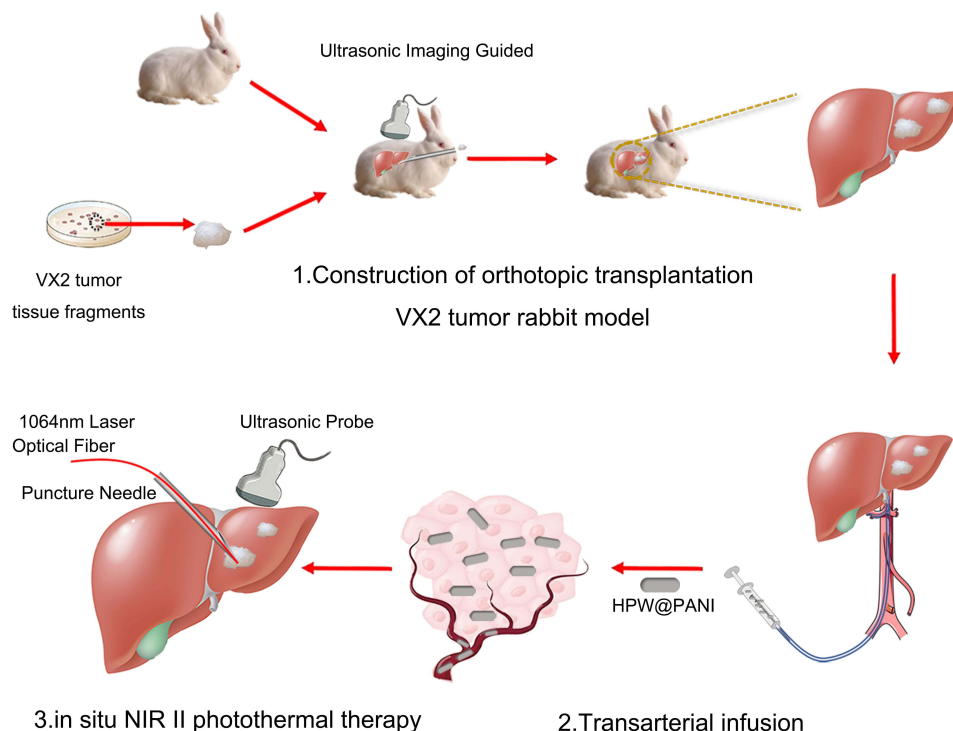
deliver drugs into the solid tumor with high dose and low systemic toxicity,[7] which has been applied in clinical therapy, such as hepatic artery infusion chemotherapy,[8–10] radioembolization,[11] transcatheter arterial chemoembolization,[12,13] and photothermal therapy of tumor.[14]

To transmit enough laser energy to the deep-buried tumors through malignant tissues deeper than 10 cm, operative exposure is a common option, which has the problem of large damage.[15] Optical fibers, which are small (few hundred micrometers in diameter), flexible, nontoxic, and chemically inert, have already proven to be valuable for in vivo clinical applications such as endoscopic procedures, illumination light guides, and laser power transmission for surgical applications.[16] Hence, we hypothesize that optical fibers could be inserted into the deep-buried tumors to transmit NIR-II laser energy to deeped buried tumors for in situ NIR-II photothermal therapy. Surprisingly, to date, no study has evaluated the efficacy of in situ NIR-II PTT based on optical fibers transmission of NIR-II laser power and transarterial infusion of NIR-II absorption nanomaterials for treatment of deep-buried tumors, urging a detailed investigation.

Recently, a variety of NIR-II absorbing nanomaterials are applied for the NIR-II photothermal treatment of tumors, including gold nanoparticles,[17,18] copper sulfide,[19,20] 2D materials,[21,22] rare-earth doped nanoparticles,[23,24] carbon nanotubes,[25,26] small organic molecular,[27,28] and conjugated polymers.[29–31] Compared with other NIR-II absorption nanomaterials, polyanilines have attracted considerable attention due to their distinctive features including strong NIR-II absorbance, desirable photothermal-conversion performance, excellent photostability, pronounced biocompatibility, as well as easy chemical modification.[32–34] PANI received special attention in various fields because of their unique π-conjugated structures, which leads to high electrical and proton conductivity in acidic conditions. Its unique redox property is suitable to facile synthesis, inexpensive fabrication, and simple and high doping chemistry. Recently, there has been more growing interest in the potential use of PANI in the field of nanomedicine, including tissue engineering, cell stimulation, or drug delivery.[35–37] The potential of PANI with strong NIR-II absorption for treatment of deep buried tumor has been largely neglected and rarely investigated. Moreover, Phosphotungstate acid is an essential member of heteropoly acid, which has been explored as an acid catalyst to degrade organic pollutants.[38] However, the insufficient

therapeutic efficiency of phosphotungstate acid makes its clinical use impractical. To tackle the aforementioned issues, aniline with phosphotungstic acid and ammonium persulphate to prepare polyaniline nanoparticles by oxidative chemical polymerized, donated as HPW@PANI Nanorods, which demonstrated strong NIR-II absorbance, excellent photostability, enhanced photothermal conversion efficiency, and good biocompatibility. Moreover, double orthotopic transplantation VX2 tumor rabbit model was fabricated, and HPW@PANI Nanorods were directly transarterial infused into primary tumor through the tumor feeding artery. Furthermore, an optical fiber was interventionally inserted into the primary VX2 tumor through a catheter to transmit 1064nm laser for in situ NIR-II PTT. In vivo experiments have proven that in situ NIR-II PTT enables the effective thermal ablation of primary tumor, inhibition of distant tumor, and suppression of peritoneal metastasis of orthotopic hepatocellular carcinoma in rabbit. Therefore, this study provides an intriguing strategy to integrate transarterial infusion of NIR-II absorption nanomaterials and in situ NIR-II PTT based on optical fibers transmission of laser power and circumvent the intrinsic limitations of conventional NIR-II PTT against deep-buried solid tumors.

Experimental Section

The Preparation of HPW@PANI Nanorods

In a typical synthesis procedure of HPW@PANI Nanorods: aniline (92μL) was added in 15mLDI water to obtain solution A. HPW (188mg) was added into 3mL DI water to provide solution B, which was kept at 4°C. $(NH_4)_2S_2O_8$ (228mg) was added into 10mL DI water to obtain solution C, which was kept at 4°C. Solution A, Solution B, and Solution C were mixed at 4°C. The mixture was kept at 4°C for 10 h. The blue solution was centrifugated under 3000 rpm to remove large particles. HPW@PANI Nanorods were obtained via centrifugation under 11,000 rpm and extensively washed with DI water and ethanol several times. The calculation of photothermal conversion efficiency, cell culture, in vitro cytotoxicity assay, in vitro photothermal ablation and statistical analysis were provided in the underline supplementary document.

Animal Models

The models of hepatocellular carcinoma (HCC) in situ and intrahepatic metastases were established in 6 rabbits with the method of ultrasound-guided percutaneous liver puncture. The VX2 tumor tissues were chopped and ground to make tumor cell suspension. VX2 tumor cell suspension (0.2 mL) was intramuscularly injected into the hind leg of the rabbit after intravenous anesthesia. After the tumor matured, the tumor tissue was removed and cut into smaller pieces with a diameter of about 0.1~0.2 cm. Firstly, after the subxiphoid region was depilated and disinfected, the left lobe parenchyma of the rabbit liver was successfully punctured with an 18G PTC needle under the guidance of ultrasound (Mindray ADP1210-01, Shenzhen, China). Secondly, the core of the needle was pulled out and the tumor tissue fragment (0.2 cm in diameter) was pushed into the liver parenchyma with the needle core. Thirdly, the needle was pulled back and punctured in another direction after the injection of the gelatin sponge. A smaller tumor fragment (0.1 cm in diameter) was pushed into the liver about 2~3 cm away from the first implanted tumor. Finally, the big tumor was defined as the primary tumor, and the smaller one was designed as the distal tumor. After the operation, the weight of the rabbits was recorded and the tumor growth was evaluated by ultrasound.

Transarterial Infusion of HPW@PANI Nanorods and in situ NIR-II PTT

On the 7th day after implantation, the activity of the tumor was evaluated by contrast-enhanced ultrasound. The contrast agent SonoVue (BraccoSulsseSA, Switzerland) was injected through the rabbit ear margin vein, and the dynamic images were acquired until the contrast agent diminished. In addition, the size and location of the tumor were evaluated by CT before treatment. When the tumor had grown to 1 cm, treatment could be started. Rabbits bearing double orthotopic transplantation VX2 tumors were randomly divided into two groups (n=3 per group): transarterial infusion of HPW@PANI Nanorods as the treatment group and transarterial infusion of PBS as the control group.

A longitudinal incision of about 3 cm was made in the right inguinal area of the anesthetized rabbit to expose the femoral artery. The distal portion of the exposed femoral artery was ligated temporarily to fill the artery. The micro-catheter (2.2F 135cm, DonghaiPharmaceutical products Co., Ltd. Japan) was flushed with heparin saline before use.

Then, the right femoral artery was punctured with a 21G puncture needle (Cook Incorporated, Bloomington. Indian, USA) visually. After the successful puncture, the micro-guide wire (Transcend, 0.014 in * 205 cm, Boston Scientific Corporation, USA) and the microcatheter were introduced into the artery successively.

Supper selection of the left hepatic artery was performed carefully, and the hepatic artery angiography was done by hand injection of contrast agent to confirm the tip of the microcatheter and the location of the tumor. HPW@PANI Nanorods (0.5 mg/mL, 8mL) were infused through the microcatheter at a rate of 48 mL/h for 10 minutes. After removing the catheter, the puncture point was pressed for 5 minutes to stop the bleeding, and the incision was stitched. Penicillin was given to fight infection after the operation.

Then, the optical fiber was introduced into orthotopic transplantation of VX2 tumor under the guidance of ultrasound guidance. Firstly, the PTC needle has penetrated the skin and tissue and reached the primary tumor in the liver under the guidance of ultrasound. Secondly, an optical fiber with 220 μm diameter was introduced into the tumor through the PTC needle after the core of which was pulled out. On the other hand, a slim temperature probe was used to monitor the temperature inside the tumor in real-time, while real-time ultrasound imaging was carried out to detect the changes in tumors during in situ NIR-II PTT.

The body weight of all rabbits was also measured and recorded before the operation and on the 3rd, and 14th days after the operation. Ultrasonography was performed on the 1st, 3rd, 5th, 7th, 10th, and 14th day after the operation, and the volume of the primary and distal tumors, as well as the number of intrahepatic metastases, were recorded. On the 14th day after the operation, all tumor-bearing rabbits were euthanized by intravenous injection of the lethal dose of simazine, then the livers were collected and photographed, and the ascites and peritoneal metastases were observed and recorded.

Immune Activation and Pathological Examination

Flow cytometry was used to analyze the immune cells in the distant tumors during HPW@PANI Nanorods-mediated in situ NIR-II PTT. The blood parameters of all the rabbits were checked before operation and after the operation. The normal liver tissue, heart, spleen, lung, and kidney of the rabbit in the experimental group were fixed with 10% formalin, paraffin-embedded sections, and hematoxylin and eosin (H&E) stained.

Apoptosicratio of VX2 Cells and Cytokine Detection

T cells were separated from spleens at control groups or in situ NIR-II PTT treatment groups and seeded in 96-well microplates with cell density at 10×10^4 cells per well (0.1 mL). VX 2 cells were added into the T cells of corresponding groups and incubated for 24 h. Then, the supernatant of T cells at different groups were collected by centrifugation. Then, the concentration of IL-2, TNF-α, IFN-γ secreted byT cells were examined by ELISA kits (obtained from Abcam) according to the specifications. The apoptosic VX2 cells were identified by FACS using Annexin V/7aad kit (obtained from Abcam) according to the specifications.

Results and Discussion
Characterization of HPW@PANI Nanorods

PANI Nanorods were prepared by oxidative chemical polymerization of aniline under phosphotungstic acid and ammonium persulphate. In a typical synthetic process, phosphotungstic acid, ammonium persulphate, and aniline were mixed, and the reaction was carried out at 4°C for 10h (Figure 1A). When the phosphotungstic acid, ammonium persulphate solution was slowly added to aniline mixture in an ice bath, the color of mixed solution changes rapidly from colorless to blue, indicating the successfully oxidation reaction. The mixtures were centrifugated to remove large particles and obtain small HPW@PANI Nanorods.

The morphologies of the HPW@PANI Nanorods were characterized using transmission electron microscopy (TEM) and dynamic light scattering (DLS) (Figure 1B and C). The average hydrodynamic size of the HPW@PANI nanorods was 178 nm, as measured using dynamic light scattering (DLS), with a polydispersity index of 0.114. The zeta potential was 15 mV (Figure S1). Moreover, no aggregation or precipitation was observed in HPW@PANI Nanorods PBS solution
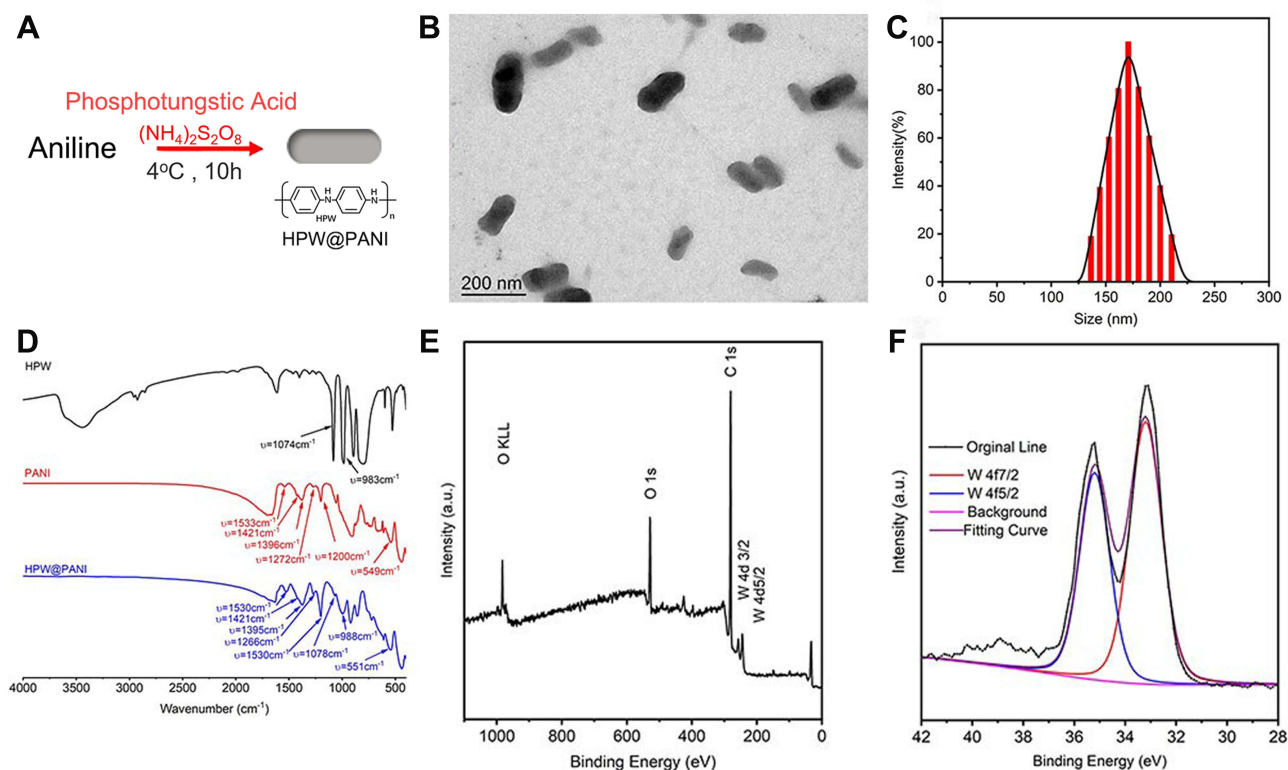
Figure 1 Characterizations of CuPW @PANI Nanorods. (**A**) The synthetic routine of HPW@PANI Nanorods. (**B**) The TEM of HPW@PANI Nanorods. (**C**) The DLS of HPW@PANI Nanorods. (**D**) The IR spectrum of HPW, PANI and HPW@PANI Nanorods. (**E**) The XPS spectrum of HPW@PANI Nanorods. (**F**) The XPS spectrum of W in HPW@PANI Nanorods.

for 22 days (Figure S2), confirming excellent stability. All these results indicated the relatively high stability of HPW@PANI Nanorods in the physiological milieu.

The HPW@PANI Nanorods was demonstrated via Fourier transform infrared (FTIR) spectroscopy. As shown in Figure 1D, the peaks of HPW@PANI Nanorods located at 1530,1396, 1207, and 551 cm^{-1} were attributed to the bonds from polyaniline. The band at 1078 and 988 cm^{-1} of HPW@PANI Nanorods was attributed to phosphotungstate acid. X-ray photoelectron spectroscopy (XPS) in Figure 1E confirmed that HPW@PANI Nanorods consist of W, O, and C elements. According to the well-resolved peaks, the two strong peaks at 35.1 eV (W 4f$_{7/2}$) and 33.2 eV (W 4f$_{5/2}$) correspond to the W (VI) valence state (Figure 1F). All these results confirm the successful fabrication of HPW@PANI Nanorods.

NIR-II Photothermal Conversion Performance of HPW@PANI Nanorods

The prepared HPW@PANI nanorods demonstrated strong optical absorption arranged from 500~1100 nm with blue color dispersed in PBS (Figure 2A). The mass extinction coefficient of HPW@PANI Nanorods was determined to be 12.53 L/g/cm at 1064 nm, which was much higher than those of TiO$_{2-x}$ (5.54 L/g.cm)[39] and SrCuSi$_4$O$_{10}$ nanosheets (2.42 L/g.cm)[40] (Figure 2B). It seems that HPW@PANINanorods can efficiently collect and convert NIR-II light energy into hyperthermia. The photothermal conversion efficiency at 1064 nm of HPW@PANI Nanorods was determined to be 57.76% (Figure 2C), which was higher than that of some previously reported conjugated polymer nanoparticles (40~53%),[41–44] the gold nano-frameworks (23.9%),[45] and MoS2 nanomaterials (43.3%).[46] Therefore, all these results verified that CuPW@PANI Nanorods are optional for NIR-II photothermal therapy. To evaluate the photothermal property of HPW@PANI Nanorods, power intensity- and time-dependent temperature enhancement of HPW@PANI Nanorods water solutions upon irradiation to 1064 nm laser were detected (Figure 2D–F). The infrared (IR) thermal images were observed using a thermal camera to analyze the corresponding temperature values (Figure S3). Upon the 1064 nm irradiation, the temperature of HPW@PANI Nanorods
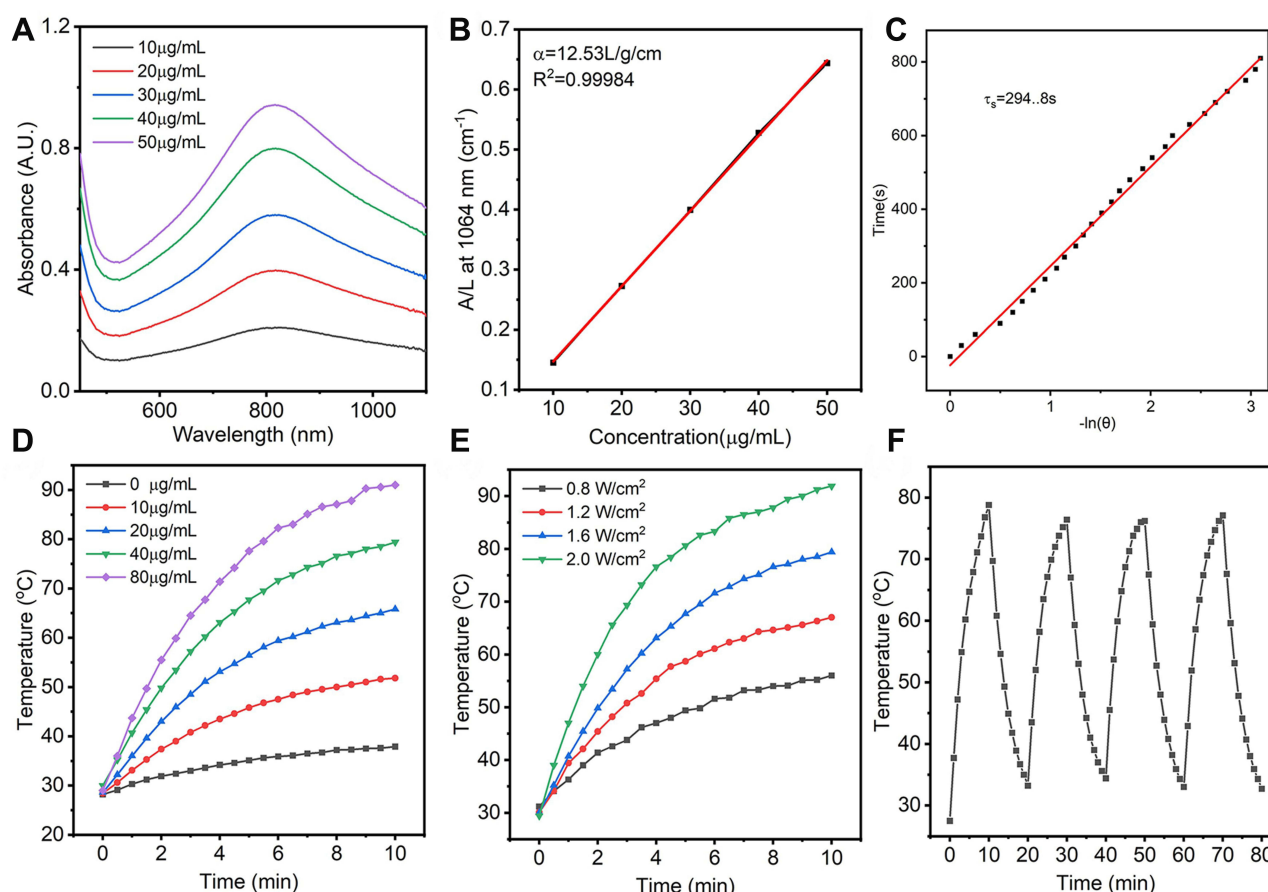
Figure 2 Photothermal conversion performance of HPW@PANI Nanorods. (**A**) The absorption spectrum of HPW@PANI nanorods with different concentration. (**B**) Fitting curve of mass extinction coefficient of HPW@PANI Nanorods at 1064 nm. (**C**) Linear time constant calculated from the cooling period. (**D**) The temperature curve of HPW@PANI Nanorods (40 μg/mL) under 1064 nm laser Irradiation with different power densities. (**E**) The temperature curve of HPW@PANI Nanorods with different concentrations under 1064 nm laser exposure (0.7 W/cm²). (**F**) Temperature rising and cooling cycles of HPW@PANI Nanorods (40 μg/mL).

solution increased quickly, while the temperature of the water slightly changed under the same condition. After 1064 nm laser (0.7 W/cm²) irradiation for 10 min, the temperature of HPW@PANI Nanorods solution enhanced about to 70 °C, which was enough to thermal ablate tumor cells. Moreover, the photothermal performance of HPW@PANI Nanorods under 1064 nm irradiation with different laser power densities was investigated. When the power density of the laser increased, HPW@PANI Nanorods solution at the same concentration generated more heat. In addition, no significant changes were observed elevating the temperature after five lasers on/off cycles irradiation, confirming the satisfactory photothermal stability of HPW@PANI Nanorods. Meanwhile, the absorption spectra of HPW@PANI Nanorods exhibited scarcely a little decline before and after exposure to 1064 nm laser for 20 min (Figure S4), indicating the excellent photothermal conversion stability of HPW@PANI Nanorods. All these results demonstrated that HPW@PANI Nanorods could efficiently translate NIR-II light energy to heat, which can be applied in NIR-II PTT.

NIR-II Photothermal Therapeutic Effect of HPW@PANI Nanorods in vitro

Considering the excellent NIR-II absorption capacity of HPW@PANI Nanorods, in vitro NIR-II photothermal anticancer efficacy was subsequently investigated. The cytotoxicity of HPW@PANI nanorods to HepG2 liver cancer cells was first evaluated. As shown in Figure 3A, when the concentration of HPW@PANI Nanorods reached 250 μg/mL, no significant cytotoxicity to HepG2 cells was observed, confirming the excellent biocompatibility of HPW@PANI Nanorods.

Next, the anticancer performance of HPW@PANI Nanorods to HepG2 cells in vitro was measured under 1064 nm irradiation. The four different treatment patterns were carried out in the in vitro NIR-II PTT experiments: (1) Control; (2) 1064 nm laser; (3) HPW@PANI Nanorods; (4) HPW@PANI Nanorods + 1064 nm laser (NIR-II PTT group). The cell
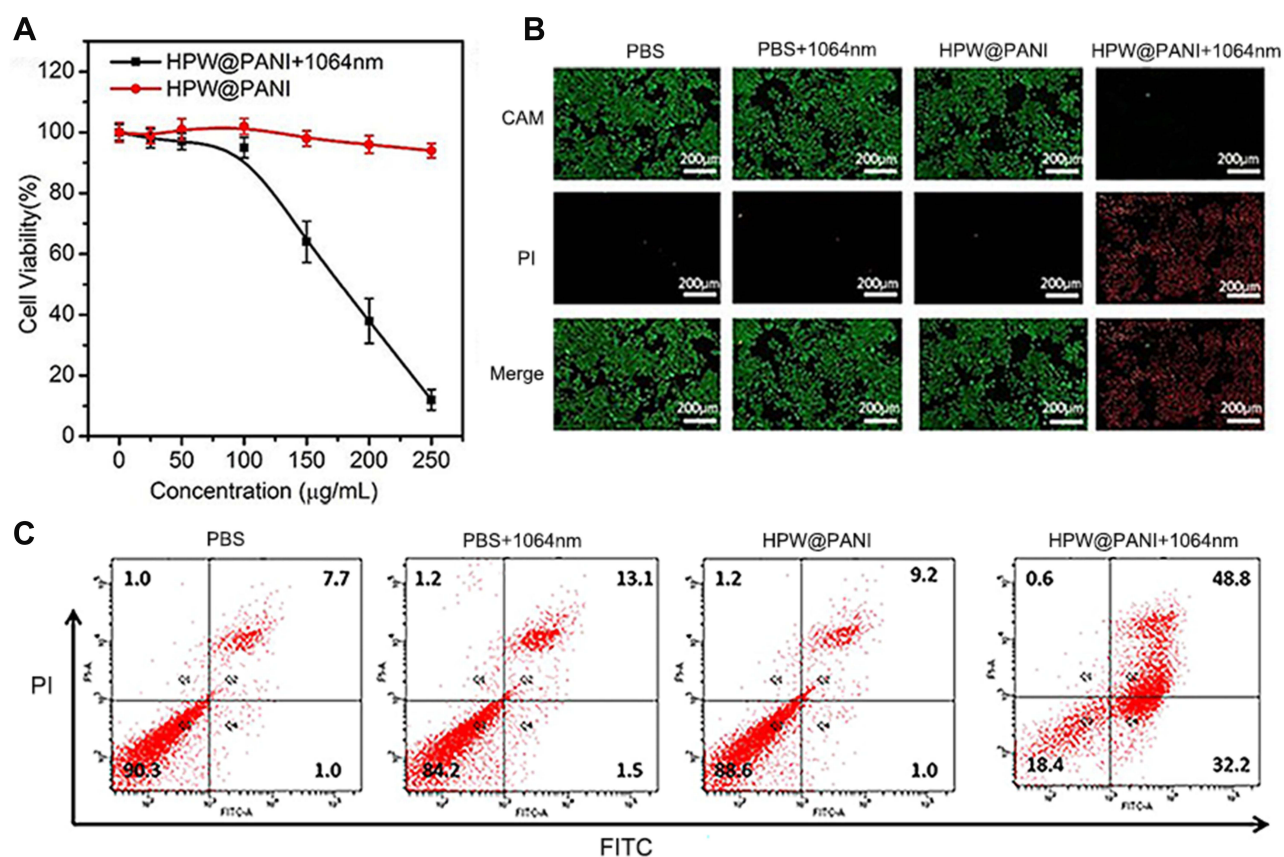
Figure 3 (**A**) The cytotoxicity of HPW@PANI Nanorods without or with 1064 nm laser irradiation. (**B**) The Live/dead staining images of HepG2 cells under different treatments. (**C**) The flow cytometric analysis of HepG2 cells under different treatments.

viabilities in the treatment pattern of (1)-(3) were higher than 90%, confirming that 1064 nm laser radiation or HPW@PANI Nanorods alone did not induce damage to HepG2 cells. However, under the treatment of HPW@PANI Nanorods plus 1064 nm laser exposure, the relative cell viability declined about 32%. These results proved the killing effect of NIR-II PTT.

Moreover, the viabilities of HepG2 cells after different treatments were visualized through live/dead co-staining, further confirming the excellent effect of NIR-II PTT in vitro. Obviously, cells treated only with HPW@PANI Nanorods or 1064 nm laser exposure exhibited bright green fluorescence with little red fluorescence. On the contrary, bright red fluorescence was observed in the cells treated by HPW@PANI Nanorods (100 μg/mL) and 1064 nm laser irradiation (0.7 W/cm^2, 5 min), which confirms the therapeutic effect of HPW@PANI Nanorods based NIR-II PTT (Figure 3B).

Finally, flow cytometry experiments were carried out to investigate the incidence of apoptosis under different treatments. As depicted in Figure 3C, the apoptotic rate of HepG2 cells treated with NIR-II PTT reached 81%, which is superior to that in treated with HPW@PANI Nanorods or 1064 nm laser irradiation alone. All these data highlighted the great treatment performance of HPW@PANI Nanorods based NIR-II PTT.

Fabrication the Orthotopic transplantationVX 2 Tumors in Rabbit

Rabbit VX2 tumor is similar to human HCC, due to the hypervascular in tumor and blood supply mainly from hepatic artery.[47,48] Moreover, the diameter of the rabbit hepatic artery is enough for catheterization in the hepatic artery. Due to these characteristics, the rabbits bearing double orthotopic transplantation VX2 tumors were fabricated for simulation the growth and metastasis of VX2 liver tumors in situ in the present study (Figure 4A). The VX2 tumor tissue fragments were transplanted into two sites in the left lobe parenchyma of the rabbit liver through the 18-gauge (G) percutaneous transhepatic cholangiography (PTC) needle under ultrasound guidance (Figure 4B). The big tumor was termed as the
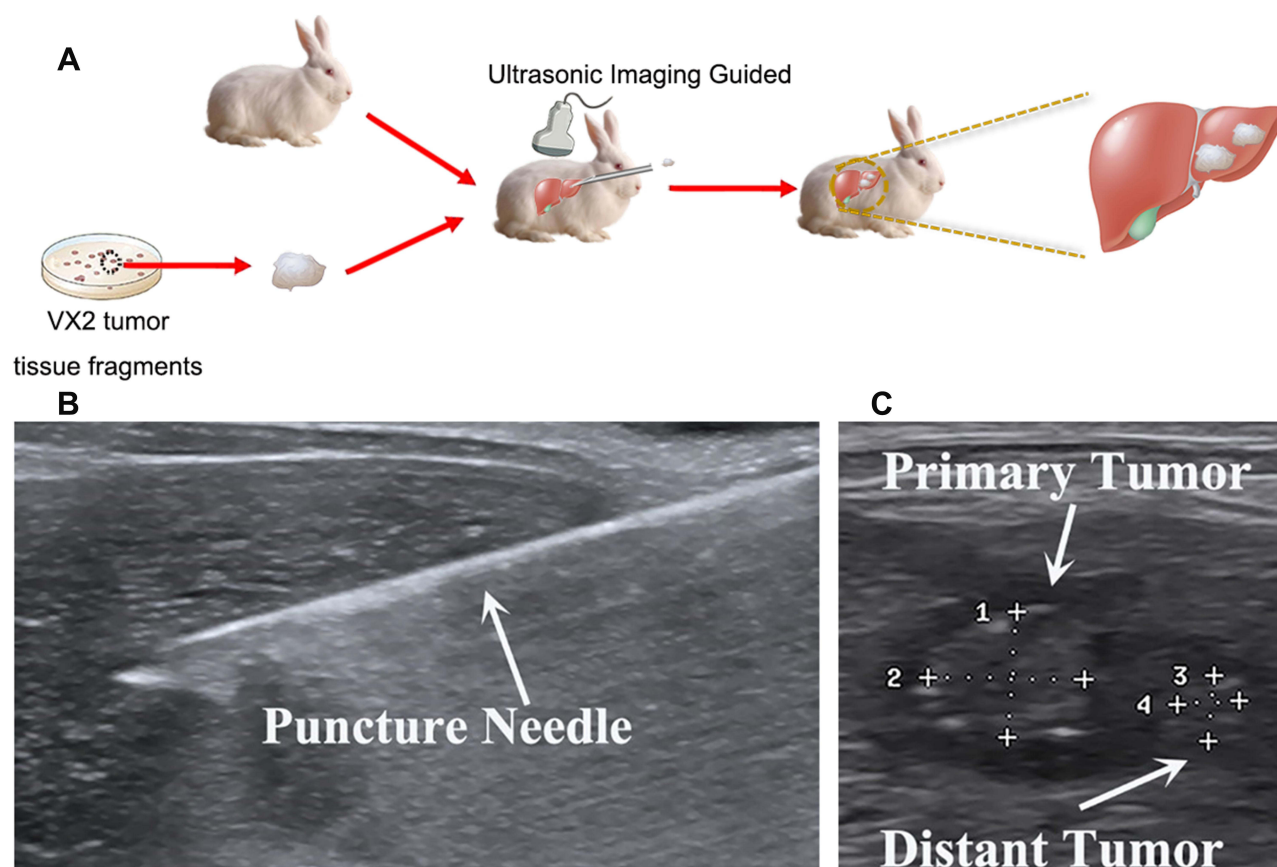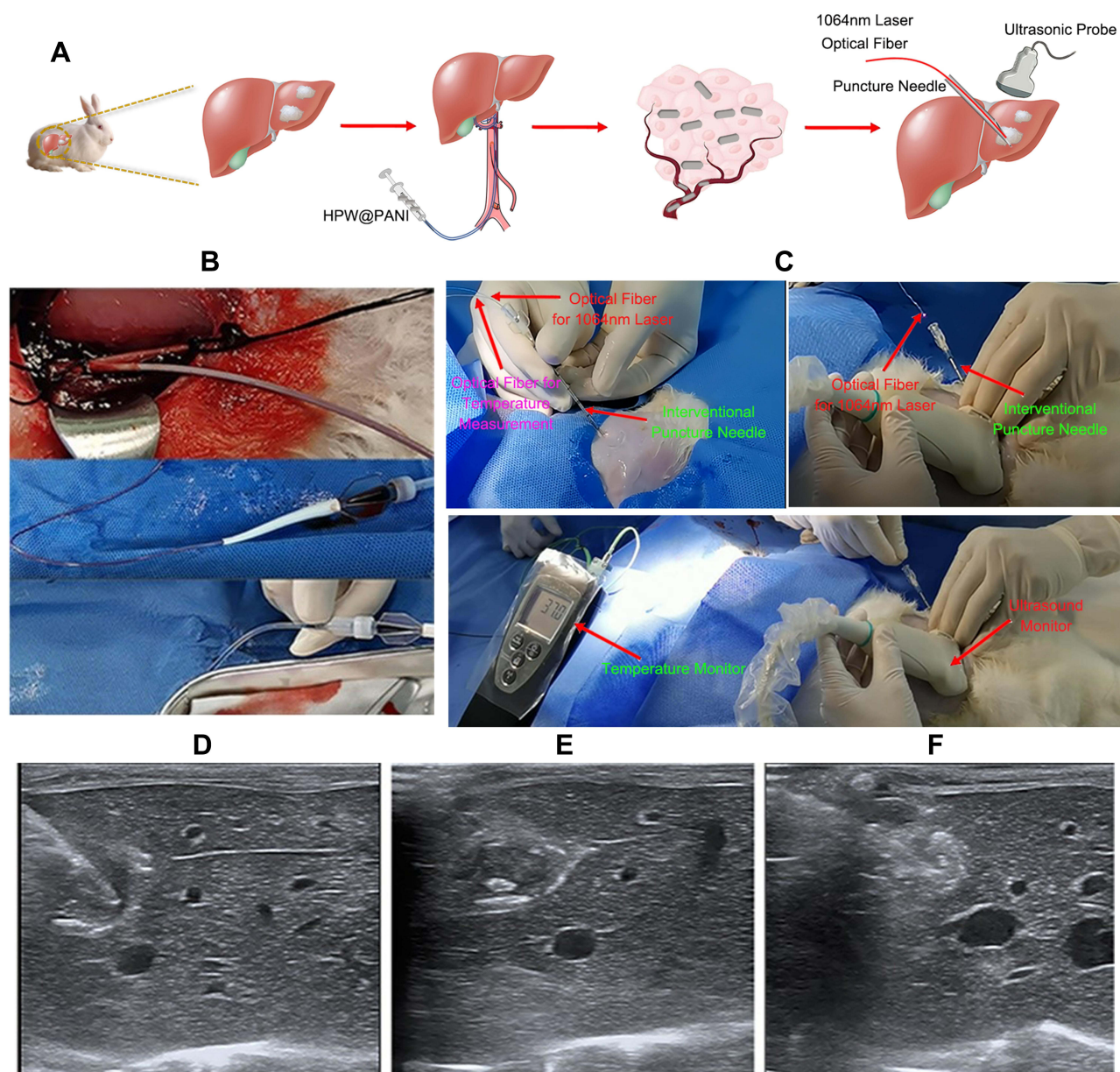
Figure 4 (**A**) Schematic illustration of the fabrication of the orthotopic transplantation VX2 tumors in the rabbit for antitumor effect. (**B**) The Ultrasonic imaging of puncture needle during orthotopic transplantation. (**C**) The Ultrasonic imaging of primary tumor and distant tumor after orthotopic transplantation.

primary tumor for in situ NIR-II photothermal therapy, while the small one was defined as the distant tumor to investigate the antitumor immunological effect (Figure 4C).

After orthotopic transplantation, ultrasonic imaging and CT imaging were carried out to confirm the successful fabrication of the double orthotopic transplantation VX2 tumor model in the rabbit. On the 7th day after inoculation, the tumors presented as uniform hypoechoic nodules under the ultrasound scan, with a clear contour and no capsule echo. During the contrast-enhanced ultrasound, the tumor showed a typical sign of "rapid wash-in and wash-out", peripheral enhancement appeared at the early arterial phase and the contrast agent faded quickly (Figure S5A). To our surprise, the feeding artery could also be seen before the peripheral enhancement. The tumor presented as a low-density mass surrounded by uniform hepatic parenchyma density with a clear boundary on CT scan (Figure S5B and S5C). During the angiography, tumor staining and peripheral neovascularization were observed in the left lobe of the liver (Figure S5D). The blood parameters results showed that there was no significant difference in serum AST and ALT between the experimental group and the control group (Figure S6). All these results confirmed the double orthotopic transplantation VX2 tumor model was successfully established. During the two-week follow-up, no rabbit died and no significant weight loss of the rabbits, which showed that this method was safe, with fewer surgical complications and no unexpected metastasis of other major organs.

Transarterial Infusion of HPW@PANINanorods and in situ NIR-II PTT

Next, HPW@PANI Nanorods were directly infused into orthotopic transplantation VX2 tumors through the tumor feeding artery (Figure 5A). The microcatheter was introduced into the left hepatic artery; HPW@PANI Nanorods were infused into the tumor through the micro-catheter with a rate of 48 mL/h for 10 minutes (HPW@PANI Nanorods 0.5mg/mL, 8mL). The color of the liquid in the catheter changed from red to blue during the infusion of HPW@PANI Nanorods as shown in Figure 5B. It seems that HPW@PANI Nanorods could be rapidly and delivered into

Figure 5 (**A**) Schematic illustration of transarterial infusion of HPW@PANI Nanorods and in situ NIRII PTT. (**B**) The photos of femoral artery catheterization and transarterial infusion of HPW@PANI Nanorods. (**C**) The photos of in situ NIR-II PTT. (**D**) Optical fiber was introduced into the tumor through the PTC needle. (**E**) and (**F**) Real-time ultrasound scanning during the treatment.

HCC tumor tissues with excellent targeting efficiency through the tumor feeding artery, resulting in high drug concentration in the solid tumor and low systemic toxicity through a greater first-pass effect in the liver, which is beneficial for real-time operation and endoscopic image guidance.

After transarterial intervention of HPW@PANI Nanorods in the primary tumor, an 18G PTC needle was used to puncture the primary tumor in the liver under the guidance of ultrasound. The optical fiber with 220 μm diameter was then inserted to the tumor through the PTC needle (Figure 5C). The 1064nm laser energy was transmitted to the primary VX2 tumor through optical fiber to generate hyperthermia. We first investigated the temperature enhancement of primary tumor after in situ 1064 nm laser irradiation. To our surprise, the temperature of primary tumor increased rapidly to 60 °C within 3 minutes, which caused tissue necrosis. However, the temperature of the surrounding normal liver parenchyma remained under 38 °C upon 1064 nm laser radiation. During the photothermal therapy, real-time ultrasound scanning showed that the hypoechoic image of the tumor was quickly replaced by the hyperechoic images, which proved that the

temperature in the tumor increased quickly (Figure 5D–F). Compared with the phototherapy therapy of the exposed liver, introducing optical fiber into the tumor in liver is feasible, accurate, and minimally invasive. Moreover, the slender temperature sensor was introduced to monitor the process of temperature rise of the tumor, which is much more accurate than the surface thermometer.[49] It seems that the introduction of optical fiber greatly improved the efficiency of photothermal ablation and decreased thermal damage to normal liver parenchyma.

Inspired by the excellent temperature enhancement in tumors induced by HPW@PANI Nanodtos under 1064nm laser radiation, in vivo experiments with the double VX2 tumor-bearing rabbit model were carried out. Rabbits bearing double orthotopic transplantation VX2 tumors were randomly divided into two groups (n=3 per group): transarterial infusion of HPW@PANI Nanorods as the treatment group and transarterial infusion of PBS as the control group. After transarterial infusion of HPW@PANI Nanorods or PBS, an optical fiber transmitted 1064nm laser energy (0.8W/cm^2, 5 min) for in situ NIR-II PTT of primary tumor. The surveillance of the primary tumors and distant tumor was recorded after 1, 3, 5, 7, 10, and 14 days by ultrasound (US) to explore the tumor development process (Figure S7 and S8). After in situ NIR-II PTT, primary tumors significantly diminished the volume or even almost vanished, which confirmed that in situ NIR-II PTT could ablate the tumors efficiently (Figure 6A and B). On the contrary, the control group exhibited no prominent antitumor effect on primary tumors. Furthermore, the volume of distant tumors significantly decreased in the treatment group, which proved that in situ NIR-II photothermal therapy could inhibit distant tumors (Figure 6C and D, and Figure S9). However, no tumor inhibition effect on distant tumor in the control group was observed. All these results confirmed that in situ NIR-II PTT treatment could ablate primary tumors and inhibit distant tumors.

Tumor metastasis is the major cause of the high tumor mortality rate, and inhibition of tumor metastasis is of significant importance for cancer treatments. On day 14, livers of both experimental and control groups were harvested to explore tumor metastasis. The tumor specimens of the control group demonstrated a fresh "fish-like" appearance, while those of the experimental group exhibited a pale hard nodule wrapped in red granulation tissue without a capsule, and most tumor centers have scorch marks due to the high temperature. Moreover, multiple large metastases were observed in the control group, while the treatment group produced few metastases (Figure 6E). The tumor tissue of the experimental group was replaced by a large number of necrotic tissues compared to that of the control group (Figure 6G). To our surprise, no significant metastasis in the peritoneum of the treated rabbit was observed. On the contrary, the rabbit in the control group produced distinct metastatic nodules in the peritoneum (Figure 6F). In short, these results confirmed that in situ NIR-II photothermal therapy based on HPW@PANI Nanorods can suppress tumor metastasis.

Studies were thus carried out to evaluate immune antitumor activity of in situ NIR-II PTT. Therefore, the ratio of CD3 +CD8+T cells in distant tumors was analyzed. Compared with control group, the tumor infiltrations of the CD3+ T cells and CD8+ T cells in in situ NIR-II PTT group were significantly increased (Figure 7A and B). This result demonstrated that in situ NIR-II PTT treatment effectively increased the infiltration of CD8+ T cells into tumor.

To further investigate the antitumor immunity of in situ NIR-II PTT, we isolated T cells from spleens in the control or in situ NIR-II PTT group and then co-cultured with VX2 cells for 24 hours in vitro. The apoptosic VX2 cells were identified by FACS using Annexin V/7aad kit and the concentration of cytokine IL-2, TNF-α, and IFN-γ super-natant were detected by ELISA kits. As shown in Figure 7C and D, it could be obviously noticed that the ratio of apoptosic cells in the treatment group was substantially higher as compared with control group. Moreover, compared with control group, a much higher level of IL-2, TNF-α, and IFNγwere induced by in situ NIR-II PTT treatment group (Figure 7E–G). As shown in Figure 7H, the IHC staining was performed on the tumors in the treatment group and the control group. Compared with the control group, the expression of Ki67 in the treatment group was significantly lower. In order to evaluate the ability of the tumor invasion and metastasis, the expression levels of N-cadherin and Vimentin were detected in this study. The results showed that the expression of N-cadherin and Vimentin in distant tumors in the treatment group was significantly down-regulated. Collectively, our results indicated that in situ NIR-II PTT can not only led to the rapid destruction of primary tumor tissue, but also stimulate specificity immunity to inhibit the growth of distant tumor and suppress peritoneal metastasis.
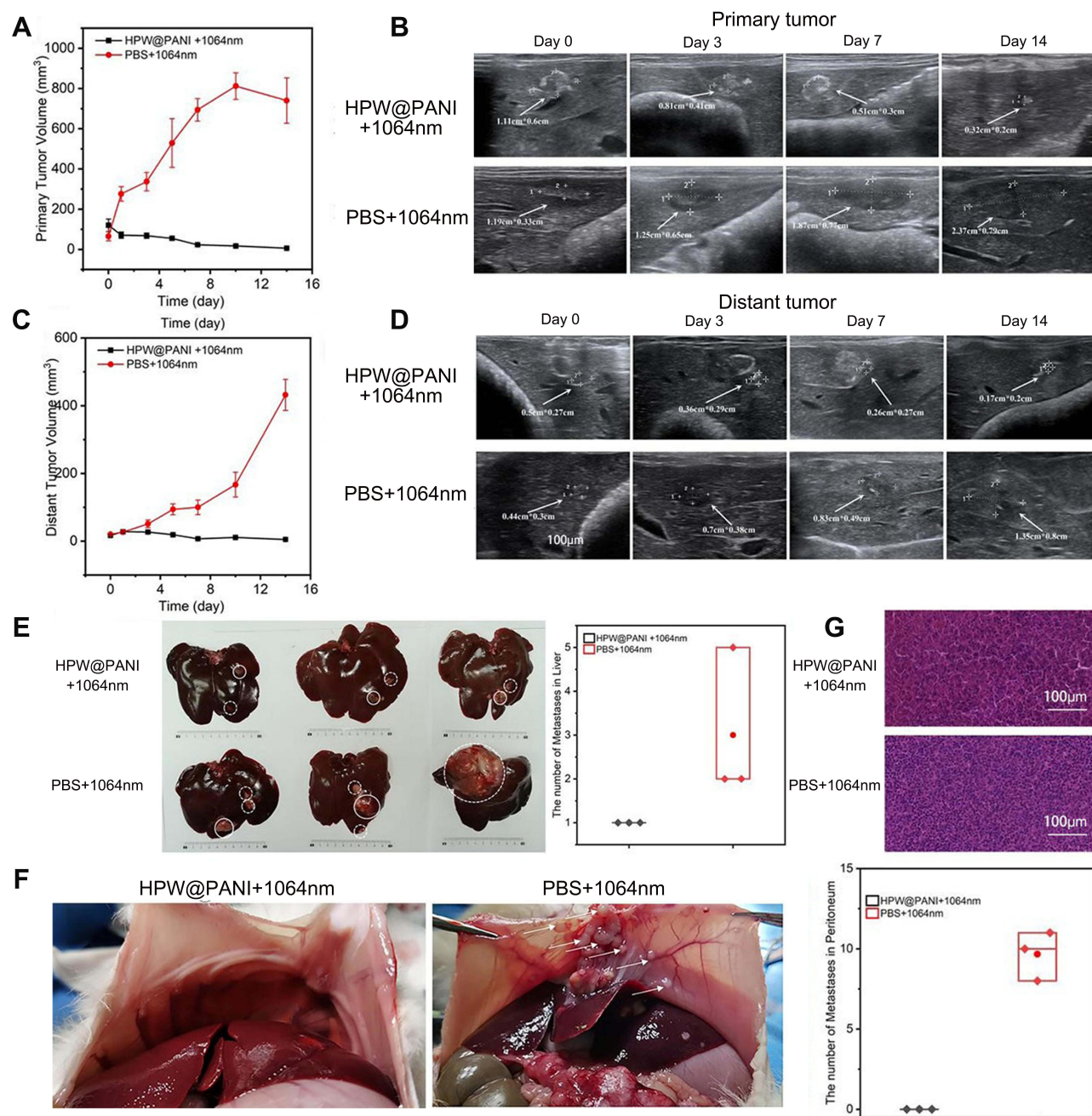
Figure 6 Antitumor effects and suppression metastasis of in situ NIR-II PTT in vivo. The tumor development process of primary tumors, (**A**) The tumor volume growth curves of primary tumors, (**B**) The ultrasonic imaging of primary tumors. (**C**) The tumor volume growth curves of distant tumors. (**D**) The ultrasonic imaging of distant tumors. (**E**) The photo and the number of metastases of the liver after different treatments. (**F**) The graph and the number of metastases of peritoneum after different treatments. (**G**) The H&E staining of tumor tissues.

Biocompability of HPW@PANINanorods

Furthermore, the potential systemic damage during HPW@PANI Nanorods mediated in situ NIR-II PTT was exploited. No distinct body weight loss was observed during in situ NIR-II PTT (Figure S10). Moreover, the main organs (heart, liver, lung, spleen, and kidney) after NIR-II PTT treatment exhibited no obvious pathological abnormalities or disorders, confirming the high biosafety of HPW@PANI Nanorods (Figure S11). In addition, blood panel analysis was carried out after transarterial infusion of HPW@PANI Nanorods (Figure S12). The blood markers, including creatinine (CR), white
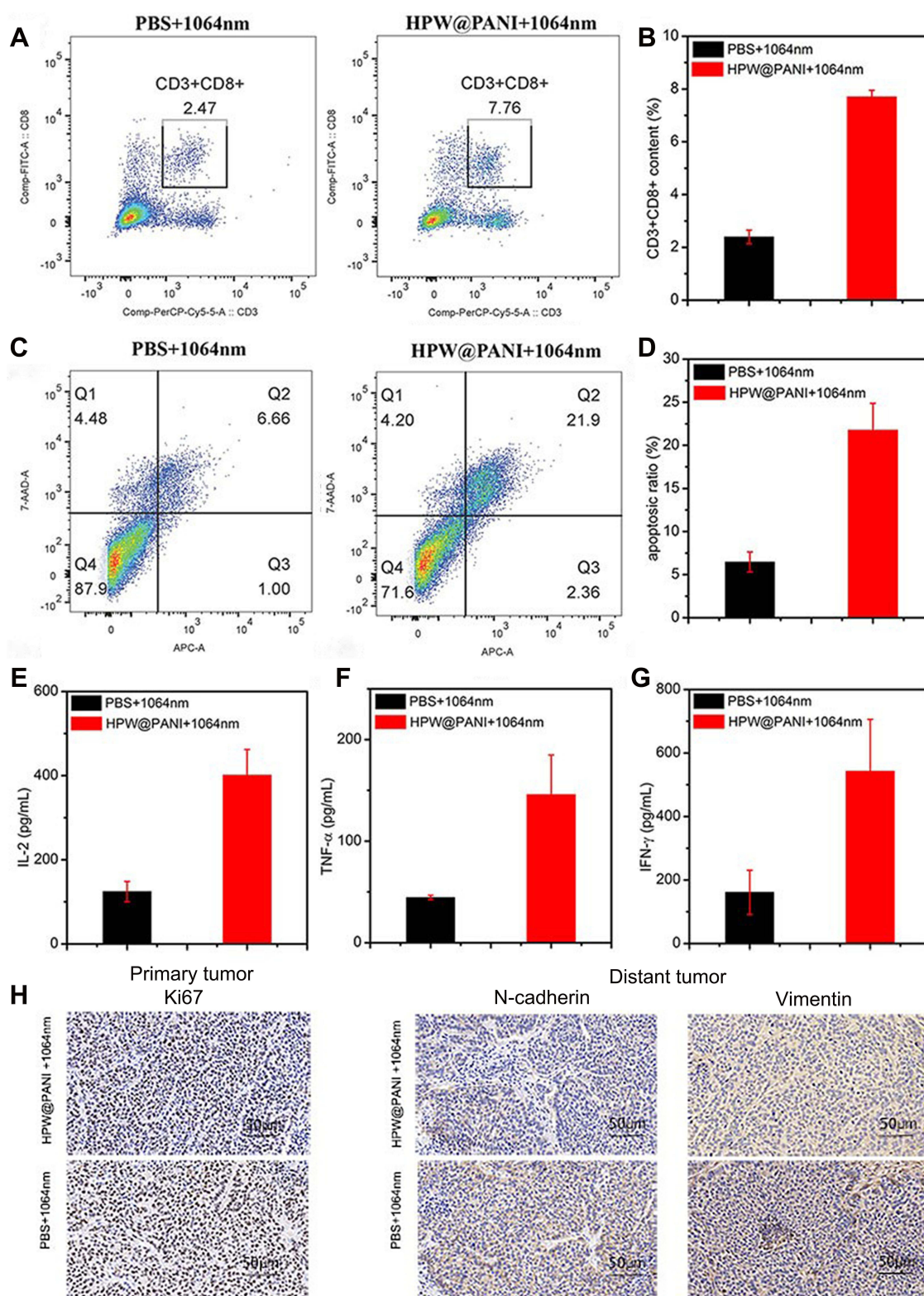
Figure 7 (**A**) Representative flow cytometry plots of CD3+ and CD8+ T cells in distant tumor after different treatment. (**B**) The proportions of CD3+ and CD8+ T cells in distant tumor after different treatment. (**C**) Representative flow cytometry plots of VX 2 cells after co-cultured with T lymphocyte stimulated from spleen from different treatment group. (**D**) The proportions of apoptotic VX2 cells after co-cultured with T lymphocyte stimulated from spleen from different treatment groups. The cytokines concentration of IL-2 (**E**), TNF-α (**F**), and IFN-γ (**G**) secreted by T lymphocyte stimulated from spleen with the VX2 cells from different treatment group. (**H**) Detection of Ki67 expression in primary tumor and N-cadherin and Vimentin expression in distant tumor were performed by IHC.

blood cells (WBC), platelets (PLT), and, hemoglobin (HGB), were within the normal reference ranges. Herein, all the above findings verified HPW@PANI Nanorods based in situ NIR-II PTT has ignorable systemic biological toxicity.

Conclusion

In conclusion, we provided a novel strategy of in situ NIR-II PTT based on optical fiber transmission of laser energy and transarterial infusion of NIR-II absorbing HPW@PANI Nanorods for treatment of orthotopic transplantation VX2 tumor in the rabbit. HPW@PANI Nanorods were prepared via oxidative chemical polymerization, which exhibited strong NIR-II absorption, higher photothermal conversion efficiency, and excellent biocompatibility. Orthotopic transplantation VX2 tumor rabbit model was fabricated, then HPW@PANI Nanorods were rapidly delivered into the VX2 tumor via transarterial infusion. Moreover, an optical fiber was inserted into in situ VX2 tumors and transmitted 1064nm laser energy for in situ NIR-II PTT. Furthermore, in vivo experiments confirmed that in situ NIR-II PTT could ablate primary tumor, inhibit distant tumor, and suppress the peritoneal metastasis. This study offers new options for improving in situ NIR-II PTT for the treatment of deep-buried solid tumors.

Ethics Statement

All animal procedures were performed in accordance with the Guidelines for Care and Use of Laboratory Animals of Southern Medical University. The present study was approved by the Nanfang hospital animal ethic committee (No: NFYY-2021-0531). Twelve New Zealand white rabbits (weighing 2.5~3 kg), aged from 2 to 3 months, were provided and raised by the Experimental Animal Center, Nanfang Hospital (China). And the HepG2 cells used in this study were purchased from China National Laboratory Cell Resource Sharing Platform.

Acknowledgments

Disclosure

The authors report no conflicts of interest in this work.

References

1. Chen S, Sun B, Miao H, et al. NIR-II dye-based multifunctional telechelic glycopolymers for NIR-iia fluorescence imaging-guided stimuli-responsive chemo-photothermal combination therapy. *ACS Mater Lett*. 2020;2(2):174. doi:10.1021/acsmaterialslett.9b00480
2. Dai H, Wang X, Shao J, et al. NIR-II organic nanotheranostics for precision oncotherapy. *Small*. 2021;2(44):2102646. doi:10.1002/smll.202102646
3. Zhen X, Pu K, Jiang X. Photoacoustic imaging and photothermal therapy of semiconducting polymer nanoparticles: signal amplification and second near-infrared construction. *Small*. 2021;17(6):2004723. doi:10.1002/smll.202004723
4. Dai R, Peng X, Lin B, Xu D, Lv R. NIR II luminescence imaging for sentinel lymph node and enhanced chemo-/photothermal therapy for breast cancer. *Bioconjug Chem*. 2021;32:2117. doi:10.1021/acs.bioconjchem.1c00393
5. Wang Y, Wang Z, Xu C, Tian H, Chen X. A disassembling strategy overcomes the EPR effect and renal clearance dilemma of the multifunctional theranostic nanoparticles for cancer therapy. *Biomaterials*. 2019;197:284. doi:10.1016/j.biomaterials.2019.01.025
6. Lin Z, Goswami N, Xue T, et al. Engineering metal nanoclusters for targeted therapeutics: from targeting strategies to therapeutic application. *Adv Funct Mater*. 2021;31:2105662. doi:10.1002/adfm.202105662
7. Zhang C, Sun W, Wang Y, et al. Gd-/CuS-loaded functional nanogels for MR/PA imaging-guided tumor-targeted photothermal therapy. *ACS Appl Mater Interfaces*. 2020;12:9107. doi:10.1021/acsami.9b23413
8. Gao L, Yan H, Zhu S, et al. Targeted delivery of Bi2Se3 Nanoflowers to orthotopic liver tumor via transarterial infusion for enhanced microwave ablation sensibilization. *Nano Today*. 2021;41:101314. doi:10.1016/j.nantod.2021.101314
9. Xie Y, Qi X, Xu K, et al. Transarterial infusion of iRGD-modified ZrO 2 nanoparticles with lipiodol improves the tissue distribution of doxorubicin and its antitumor efficacy. *J VascInterv Radiol*. 2019;30:2026. doi:10.1016/j.jvir.2019.04.014
10. Zhang Y-Q, Jiang L-J, Jiang S-X, et al. Gefitinib with or without transarterial infusion chemotherapy (cisplatin) for large nonsmall cell lung cancer with epidermal growth factor receptor mutations. *J VascInterv Radiol*. 2019;30:1004.
11. Anteby R, Kemeny NE, Kingham TP, et al. Getting chemotherapy directly to the liver: the historical evolution of hepatic artery chemotherapy. *J Am Coll Surg*. 2021;232(3):332. doi:10.1016/j.jamcollsurg.2020.11.013
12. Li R, Li D, Jia G, Li X, Sun G, Zuo C. Diagnostic performance of theranostic radionuclides used in transarterial radioembolization for liver cancer. *Front Oncol*. 2021;10:551622. doi:10.3389/fonc.2020.551622
13. Vogl TJ, Gruber-Rouh T. HCC: transarterial therapies-what the interventional radiologist can offer. *Dig Dis Sci*. 2019;64(4):959. doi:10.1007/s10620-019-05542-5

14. Pang H, Tian C, He G, et al. NIR-absorbing Prussian blue nanoparticles for transarterial infusion photothermal therapy of VX2 tumors implanted in rabbits. *Nanoscale*. 2021;13(18):8490. doi:10.1039/D1NR01394G

15. Abbass MA, Ahmad SA, Mahalingam N, et al. In vivo ultrasound thermal ablation control using echo decorrelation imaging in rabbit liver and VX2 tumor. *PLoS One*. 2019;14(12):0226001. doi:10.1371/journal.pone.0226001

16. Katzir A. optical fiber techniques for medical applications. In: Meyers RA, editor. *Encyclopedia of Physical Science and Technology*. 3rd ed. Academic Press; 2003:315–333.

17. Shen J, Karges J, Xiong K, et al. Cancer cell membrane camouflaged iridium complexes functionalized black-titanium nanoparticles for hierarchical-targeted synergistic NIR-II photothermal and sonodynamic therapy. *Biomaterials*. 2021;275:120979. doi:10.1016/j.biomaterials.2021.120979

18. Tabish TA, Dey P, Mosca S, et al. Smart gold nanostructures for light mediated cancer theranostics: combining optical diagnostics with photothermal therapy. *Adv Sci*. 2020;7(15):1903441. doi:10.1002/advs.201903441

19. Hu R, Fang Y, MI. H, et al. Ultrasmall Cu 2-x S nanodots as photothermal-enhanced Fenton nanocatalysts for synergistic tumor therapy at NIR-II biowindow. *Biomaterials*. 2019;206:101. doi:10.1016/j.biomaterials.2019.03.014

20. Wang S, Hu T, Wang G, et al. Ultrathin CuFe2S3 nanosheets derived from CuFe-layered double hydroxide as an efficient nanoagent for synergistic chemodynamic and NIR-II photothermal therapy. *Chem Eng J*. 2021;419:129458. doi:10.1016/j.cej.2021.129458

21. Zhang Q, Guo Q, Chen Q, et al. Highly efficient 2D NIR-II photothermal agent with fenton catalytic activity for cancer synergistic photothermal-chemodynamic therapy. *Adv Sci*. 2020;7(7):1902576. doi:10.1002/advs.201902576

22. An D, Fu J, Zhang B, et al. NIR-II responsive inorganic 2D nanomaterials for cancer photothermal therapy: recent advances and future challenges. *Adv Funct Mater*. 2021;31(32):2101625. doi:10.1002/adfm.202101625

23. Jiang M, Liu H, Zeng S, Hao J. A general in situ growth strategy of designing theranostic NaLnF 4 @Cu 2− x S nanoplatform for in vivo NIR-II optical imaging beyond 1500 nm and photothermal therapy. *Adv Therap*. 2019;2(6):1800153. doi:10.1002/adtp.201800153

24. Xiang H, Lin H, Yu L, Chen Y. Hypoxia-irrelevant photonic thermodynamic cancer nanomedicine. *ACS Nano*. 2019;13(2):2223. doi:10.1021/acsnano.8b08910

25. Li Y, Bai G, Zeng S, Hao J. Theranostic carbon dots with innovative NIR-II emission for in vivo renal-excreted optical imaging and photothermal therapy. *ACS Appl Mater Interfaces*. 2019;11(5):4737. doi:10.1021/acsami.8b14877

26. Geng B, Qin H, Shen W, et al. Carbon dot/WS2 heterojunctions for NIR-II enhanced photothermal therapy of osteosarcoma and bone regeneration. *Chem Eng J*. 2020;383:123102. doi:10.1016/j.cej.2019.123102

27. Jiang Z, Zhang C, Wang X, et al. A borondifluoride-complex-based photothermal agent with an 80 % photothermal conversion efficiency for photothermal therapy in the NIR-II window. *Angew Chem Int Ed*. 2021;60(41):22376. doi:10.1002/anie.202107836

28. Tang B, Li W-L, Chang Y, et al. A supramolecular radical dimer: high-efficiency NIR-II photothermal conversion and therapy. *Angew Chem Int Ed*. 2019;58(43):15526. doi:10.1002/anie.201910257

29. Yin C, Li X, Wang Y, et al. Organic semiconducting macromolecular dyes for NIR-II photoacoustic imaging and photothermal therapy. *Adv Funct Mater*. 2021;31(37):2104650. doi:10.1002/adfm.202104650

30. Xu C, Jiang Y, Han Y, Pu K, Zhang R. A polymer multicellular nanoengager for synergistic NIR-II photothermal immunotherapy. *Adv Mater*. 2021;33(14):2008061. doi:10.1002/adma.202008061

31. Li J, Jiang R, Wang Q, et al. Semiconducting polymer nanotheranostics for NIR-II/Photoacoustic imaging-guided photothermal initiated nitric oxide/photothermal therapy. *Biomaterials*. 2019;217:119304. doi:10.1016/j.biomaterials.2019.119304

32. Zhang Y, Wang Y, Yang X, Yang Q, Li J, Tan W. Polyaniline nanovesicles for photoacoustic imaging-guided photothermal-chemo synergistic therapy in the second near-infrared window. *Small*. 2020;16(35):2001177. doi:10.1002/smll.202001177

33. Yan L-X, Chen L-J, Zhao X, Yan X-P. pH switchable nanoplatform for in vivo persistent luminescence imaging and precise photothermal therapy of bacterial infection. *Adv Funct Mater*. 2020;30(14):1909042. doi:10.1002/adfm.201909042

34. Tian Q, Li Y, Jiang S, et al. Tumor pH-responsive albumin/polyaniline assemblies for amplified photoacoustic imaging and augmented photothermal therapy. *Small*. 2019;15(42):1902926. doi:10.1002/smll.201902926

35. Chiou NR, Lu C, Guan L, Lee J, Epstein AJ. Growth andAlignment of polyaniline nanofibres with superhydrophobic, superhydrophilic and other properties. *Nat Nanotechnol*. 2007;2(6):354–357. doi:10.1038/nnano.2007.147

36. Gospodinova N, Terlemezyan L. Conducting polymers prepared by oxidative polymerization: polyaniline. *Prog Polym Sci*. 1998;23(8):1443–1484. doi:10.1016/S0079-6700(98)00008-2

37. Bhadra S, Khastgir D, Singha NK, Lee JH. Progress inPreparation, processing and applications of polyaniline. *Prog Polym Sci*. 2009;34:783–810.

38. Chen JS, Sankar A, Lin YJ, et al. Phosphotungstic acid as a novel acidic catalyst for carbohydrate protection and glycosylation. *RSC Adv*. 2019;9 (58):33853–33862. doi:10.1039/C9RA06170C

39. Han XX, Huang J, Jing XX, et al. Oxygen-deficient black titania for synergistic/enhanced sonodynamic and photoinduced cancer therapy at near infrared-II biowindow. *ACS Nano*. 2018;12:4545. doi:10.1021/acsnano.8b00899

40. Yang C, Younis MR, Zhang J, Qu J, Lin J, Huang P. Programmable NIR-II photothermal-enhanced starvation-primed chemodynamic therapy using glucose oxidase-functionalized ancient pigment nanosheets. *Small*. 2020;16:2001518. doi:10.1002/smll.202001518

41. Sun P, Jiang X, Sun B, et al. Electron-acceptor density adjustments for preparation conjugated polymers with NIR-II absorption and brighter NIR-II fluorescence and 1064 nm active photothermal/gas therapy. *Biomaterials*. 2022;208:121319. doi:10.1016/j.biomaterials.2021.121319

42. Jiang Y, Li J, Zhen X, Xie C, Pu K. Dual-peak absorbing semiconducting copolymer nanoparticles for first and second near-infrared window photothermal therapy: a comparative study. *Adv Mater*. 2018;30:1705980. doi:10.1002/adma.201705980

43. Cheng Q, Tian Y, Dang H, et al. Antiquenching macromolecular NIR-II probes with high-contrast brightness for imaging-guided photothermal therapy under 1064 nm irradiation. *Adv Healthcare Mater*. 2021;11:2101697. doi:10.1002/adhm.202101697

44. Yin C, Tai X, Li X, et al. Side chain engineering of semiconducting polymers for improved NIR-II fluorescence imaging and photothermal therapy. *Chem Eng J*. 2022;428:132098. doi:10.1016/j.cej.2021.132098

45. Wang JP, Sun JY, Wang YH, et al. Gold nanoframeworks with mesopores for raman-photoacoustic imaging and photo-chemo tumor therapy in the second near-infrared biowindow. *Adv Funct Mater*. 2020;30:1908825. doi:10.1002/adfm.201908825

46. Zhou Z, Li BW, Shen C, et al. Metallic 1T phase enabling MoS2 nanodots as an efficient agent for photoacoustic imaging guided photothermal therapy in the near-infrared-II window. *Small*. 2020;16:2004173. doi:10.1002/smll.202004173

47. Khabbaz RC, Huang YH, Smith AA, et al. Development and angiographic use of the rabbit VX2 model for liver cancer. *J Vis Exp*. 2019;143: e58600.

48. Yi HM, Cai BH, Ai X, Li KY, Zhang W. Establishment of rabbit liver VX2 tumor model using percutaneous puncture inoculation of tumor fragment guided and evaluated by ultrasonography. *Curr Med Sci*. 2019;39:820. doi:10.1007/s11596-019-2111-6

49. Zhou J, Ling G, Cao J, et al. Transcatheter intra-arterial infusion combined with interventional photothermal therapy for the treatment of hepatocellular carcinoma. *Int J Nanomedicine*. 2020;15:1373. doi:10.2147/IJN.S233989